

Structural and functional characterization of human Iba proteins

Jörg O. Schulze¹, Claudia Quedenau², Yvette Roske¹, Thomas Adam³, Herwig Schüler¹, Joachim Behlke¹, Andrew Turnbull¹, Volker Sievert², Christoph Scheich², Uwe Mueller⁴, Udo Heinemann^{1,5} and Konrad Büssow^{2,6}

1 Max Delbrück Center for Molecular Medicine, Berlin, Germany

2 Max Planck Institute for Molecular Genetics, Berlin, Germany

3 Institute of Microbiology and Hygiene, Charité Medical School, Berlin, Germany

4 Macromolecular Crystallography, BESSY GmbH, Berlin, Germany

5 Institute of Chemistry and Biochemistry – Crystallography, Free University, Berlin, Germany

6 Department of Structural Biology, Helmholtz Centre for Infection Research, Braunschweig, Germany

Correspondence:

Udo Heinemann, MDC, Robert-Rössle-Str. 10, 13125 Berlin, Germany

Fax: +49 30 9406 2548

Tel: +49 30 9406 3420

E-mail: heinemann@mdc-berlin.de

Konrad Büssow, HZI, Inhoffenstr. 7, 38124 Braunschweig, Germany

Fax: +49 531 6181 7099

Tel: +49 531 6181 7064

E-mail: konrad.buessow@helmholtz-hzi.de

Running title: Human Iba proteins

Abbreviations:

CFP, cyan fluorescent protein; DAPI, 4',6-diamidino-2-phenylindol; DTT, dithiothreitol; Iba, ionized calcium binding adapter molecule; TCEP, tris(2-carboxyethyl) phosphine; TEV, tobacco etch virus; YFP, yellow fluorescent protein.

Keywords:

ionized calcium binding adapter molecule, allograft inflammatory factor 1, actin crosslinking, EF-hand, calcium binding

Summary

Iba2 is a homolog of ionized calcium binding adapter molecule 1 (Iba1), a 17 kDa protein that binds and crosslinks filamentous actin (F-actin) and localizes to membrane ruffles and phagocytic cups. Here, we present the crystal structure of human Iba2 and its homodimerization properties, F-actin crosslinking activity, cellular localization and recruitment upon bacterial invasion in comparison with Iba1. The Iba2 structure comprises two central EF-hand motifs lacking bound Ca^{2+} . Iba2 crystallized as a homodimer stabilized by a disulfide bridge and zinc ions. Analytical ultracentrifugation revealed a different mode of dimerization under reducing conditions that was independent of Ca^{2+} . Furthermore, no binding of Ca^{2+} up to 0.1 mM was detected by equilibrium dialysis. Correspondingly, Iba EF-hand motifs lack residues essential for strong Ca^{2+} coordination. Sedimentation experiments and microscopy detected pronounced, indistinguishable F-actin binding and crosslinking activity of Iba1 and Iba2 with induction of F-actin bundles. Fluorescent Iba fusion proteins were expressed in HeLa cells and colocalized with F-actin. Iba1 was recruited into cellular projections to a larger extent than Iba2. Additionally, we studied Iba recruitment in a *Shigella* invasion model that induces cytoskeletal rearrangements. Both proteins were recruited into the bacterial invasion zone and Iba1 was again concentrated slightly higher in the cellular extensions.

Introduction

Iba1, also known as allograft inflammatory factor 1 (AIF-1), is a 17 kDa protein with a central pair of EF-hand motifs [1]. This feature is common to a large family of Ca^{2+} -binding proteins known as EF-hand proteins [2]. Iba1 was found to bind calcium ions in overlay assays [3]. The structure of human Iba1 (h-Iba1) was determined by X-ray crystallography (PDB code 2d58) [4] and NMR (unpublished; PDB code 2G2B). Both techniques revealed a monomeric, Ca^{2+} -free protein. However, the crystal structure of Iba1 from mouse (m-Iba1; PDB code 1wy9) showed a homodimeric protein with Ca^{2+} bound to only the second EF-hand motif [4]. Thus, the dimerization of Iba1 was suggested to be induced by Ca^{2+} binding.

A homolog of Iba1 named C9orf58 or Iba2 was revealed by the Human Genome Project. Human Iba2 consists of 150 amino acids (17kDa), and the sequence identity to h-Iba1 is 60%. A systematic microarray study has revealed expression profiles for most of the human transcripts and uncovered different tissue specific expression of Iba1 and Iba2 [5]. For Iba1, a preferential expression in spleen, tonsil, lymph node, thymus and also lung was found, confirming previous results [6, 7]. A pronounced expression in the kidney was found for Iba2. Iba1 is upregulated in mononuclear cells found in transplanted hearts in the course of allograft rejection [7, 8] and in heart arteries injured by balloon angioplasty [6]. Iba1 expression in vascular smooth muscle cells (VSMC) is induced upon tissue injury by cytokines [9]. Iba1 expression was examined in mouse by comprehensive immunohistochemistry. All subpopulations of macrophages were positive, except for alveolar macrophages [10]. Spermatids were the only cells not belonging to the monocyte/macrophage lineage expressing Iba1 [10]. Organized actin cytoskeleton remodeling is essential for macrophages and Iba1 was found to bind and crosslink filamentous actin (F-actin) [11, 12] and to translocate to lamellipodia, membrane ruffles and phagocytic cups [3, 12]. Iba1 cooperates with L-fimbrin, another F-actin-bundling protein, as it was shown to directly bind fimbrin and to enhance its activity [13].

This study is the result of a systematic analysis of proteins [14] encoded by clones of the German cDNA Consortium [15]. LIFEdb, a database integrating systematic studies with this cDNA collection, includes information on the subcellular localization of the corresponding proteins [16, 17]. LIFEdb reports colocalization with the cytoskeleton and adhesion plaques for the Iba2 cDNA clone DKFZp761J191 derived protein.

The structure presented here reveals functional similarities and differences between Iba1 and Iba2. We investigated Ca^{2+} binding and homodimerization of Iba1 and Iba2. Furthermore, F-

actin binding and crosslinking assays were performed with both human Iba proteins, and their role in bacterial invasion was investigated.

Results

Crystal structures of Iba2

Human Iba2 crystallized in two different crystal forms under the same conditions. The first crystal form (Iba2_t) grew in the trigonal space group P3₂21 and contained one molecule per asymmetric unit. The second form (Iba2_o) crystallized in the orthorhombic space group P2₁2₁2 with four molecules in the asymmetric unit (Table 1). The Iba2 structure was solved by molecular replacement using m-Iba1 (PDB-code 1WY9) [4] as a search model, which shares a sequence identity of 60% with Iba2. The crystal structure of Iba2_t was refined to a maximal resolution of 2.45 Å while Iba2_o was refined to 2.15 Å.

Iba2 is a compact, single-domain protein composed mainly of α -helices (Fig. 1, 2). The core of Iba2 is a pair of EF-hand motifs, denoted as EF-hands 1 and 2, each consisting of two α -helices (α A, α B and α C, α D, respectively) flanking a loop region able to bind calcium ions in EF-hand proteins [18]. As commonly observed in EF-hand proteins [18], the two motifs have an approximately two-fold rotation symmetry with a pseudo-dyad axis passing through the small anti-parallel β -sheet in the center. Despite extensive efforts, no crystal structure with calcium ions bound to the EF-hands could be obtained. Two additional helices (α N and α E) complement the EF-hand pair on both termini. 12 residues at the N-terminus and 23 residues at the C-terminus are not visible in the final electron density maps of the five Iba2 molecules observed in total. Thus, the termini are either flexible or degraded. All five molecules show basically the same conformation with root mean square deviations (r.m.s.d.) of C α atoms ranging from 0.77 to 0.91 Å. In one molecule of Iba2_o, however, the residues 74 - 90 of the helix-loop-helix region α B- α C are not resolved.

The overall topology of Iba2 shows structural similarities to classical EF-hand proteins. The second pair of EF-hands in calmodulin (PDB code 1CLL) [19] and the second pair of EF-hands in troponin C (PDB code 1NCX) [20] are structurally closely related to Iba2. The corresponding DALI Z-scores are 8.2 and 7.2, respectively. As expected, h-Iba1 [4] is structurally most closely related to Iba2 (Z-score 13.4).

Unusual dimerization of Iba2

In crystal form Iba2_t, which contains one monomer per asymmetric unit, a homodimer is assembled that contains a central disulfide bridge between Cys35 residues of adjacent molecules related by crystallographic symmetry along a two-fold rotation axis (Fig. 2). This dimer is stabilized further by the coordination of two Zn²⁺ ions by Glu28 and Glu43 side chains in the dimerization interface. Zn²⁺ was provided by the crystallization solution, which contained 100 mM zinc acetate. Nevertheless, the dimerization interface is relatively small and includes only three hydrogen bonds between the dimer subunits. The interface comprises approximately 360 Å² corresponding to only 5% of the total solvent accessible surface area of one Iba2 molecule.

Crystal form Iba2_o, with its four molecules in the asymmetric unit contains two similar homodimers, which are formed by non-crystallographic symmetry in this case. These two dimers feature identical Cys35-Cys35' disulfide bridges as observed in crystal form Iba2_t. Moreover, there is only one Zn²⁺ ion bound in each dimerization interface of Iba2_o and the Zn²⁺ ions are additionally coordinated by His85 side chains of adjacent molecules. There are two additional Zn²⁺ ions bound by the Glu64 and Asp107 side chains of adjacent molecules as well as by the Glu32 side chains of neighbouring molecules along a two-fold rotation axis. These ions form stabilizing crystal contacts, but are not located in potential dimerization or oligomerization interfaces.

Dimerization in solution

Purification of Iba2 was always performed in the presence of a reducing agent, dithiothreitol (DTT). SDS-PAGE without prior reduction confirmed the absence of disulfide bonds in purified Iba2 (data not shown). However, formation of a disulfide-bridged dimer by oxidation was observed upon removal of DTT and incubation at room temperature. It is likely that the disulfide bond in the Iba2 structures formed during crystallization after the DTT in the buffer had been oxidized. Analytical ultracentrifugation showed that human Iba1 and Iba2 form homodimers under reducing conditions with dissociation constants of approximately 150 and 20 μM, respectively (Fig. 3). The presence of Ca²⁺ had only a marginal effect on the dimerization of both Iba proteins.

F-actin binding and crosslinking

Iba1 is known to bind and crosslink actin polymers [12]. We found that both Iba1 and Iba2 co-sedimented to a similar extent with actin polymers in ultracentrifugation experiments (Fig. 4A). Removal of Ca^{2+} by EGTA had no effect on the co-sedimentation of Iba1 and Iba2.

Actin polymers alone do not sediment during centrifugation at $8,000\times g$ (Fig. 4B). When added at 0.1:1 molar ratio, both Iba1 and Iba2 efficiently shifted F-actin into low-speed pellets, indicating extensive F-actin crosslinking. This effect was even stronger at higher molar ratios. Ca^{2+} dependence of the crosslinking activity was not tested.

Actin polymers specifically stained with a fluorescent phalloidin analog appear as a loose network of thin fibers with occasional formation of bundles (Fig. 5A). Bundle formation differs between actin isoforms and is a function of polymer concentration and ionic strength [21]. At 0.1:1 molar ratio, both Iba proteins completely abolish the background of thin actin fibers and crosslink all actin polymers into bundles (Fig. 5B-C). There are no apparent differences in the filament-crosslinking efficiency of Iba1 and Iba2 or in the overall morphology of the generated filament bundles.

Calcium affinity of Iba1 and Iba2

Homodimerization and actin binding of Iba1 and Iba2 were similar in the absence or presence of calcium ions. Calcium binding in solution was assayed by equilibrium dialysis. Iba1, Iba2 and calmodulin as positive control were dialyzed against a CaCl_2 solution that was labelled by a trace amount of radioactive $^{45}\text{CaCl}_2$.

When protein samples are subjected to equilibrium dialysis, they end up with the same concentration of free ligand molecules as in the dialysis buffer and with additional ligand molecules bound to the protein. An increased Ca^{2+} concentration was observed in the dialyzed calmodulin sample due to binding of Ca^{2+} (Fig. 6). No calcium binding was observed for Iba1 and Iba2.

Cellular localization and recruitment to sites of *Shigella* invasion

We expressed CFP-tagged Iba2 in HeLa cells and found that the construct colocalized with F-actin (Fig. 7A-C), in particular with subcortical filaments. Iba2 was also found in cellular projections and adhesion structures, but it was less concentrated in these structures. Recruitment of human YFP-tagged Iba1 into cell adhesion plaques and cellular projections was more pronounced in comparison (Fig. 7D-F).

In order to verify these potential differences in recruitment patterns of Iba isoforms, we studied Iba recruitment in a *Shigella* invasion model known to induce major cytoskeletal

rearrangements [22]. Here, we show that both Iba proteins are recruited into the bacterial invasion zone. Again, Iba2 seemed to be less concentrated in membrane ruffle-like cellular protrusions (Fig. 8A-D) compared with Iba1 (Fig. 8E-H). In order to verify this relatively subtle difference in protein recruitment behaviour of the two Iba proteins, we studied both Iba1 and Iba2 constructs in individual cells. We therefore double-transfected HeLa cells with both Iba constructs, infected the cells and obtained Iba1- or Iba2-specific recruitment patterns in individual cells. As shown in Fig. 8I-L, *Shigella*-induced Iba2 recruitment into cellular protrusions was less pronounced than the Iba1 pattern.

Discussion

Structural comparison of Iba2 with Iba1

Structurally, the Iba2 monomer is very similar to monomeric h-Iba1 [4] (Fig. 9A). The r.m.s.d. of common C_{α} atom positions is 1.5 Å. The two structures differ significantly only in the conformation of EF-hand 2 (as discussed below).

Dimeric m-Iba1 [4], on the other hand, deviates more from Iba2 as substantiated by an r.m.s.d. of 4.2 Å. There is an overall conformational rearrangement including a positional shift of helices αB and αC (Fig. 9B). But most notably, the C-terminal helix αE is relocated by up to 15 Å for residue Ile117 of m-Iba1 (black arrow in Fig. 9B). This dramatic rearrangement opens the dimerization interface and enables the tight interaction of the subunits in the m-Iba1 homodimer. It was suggested that the movement of αE is induced by Ca^{2+} binding to EF-hand 2 [4].

The three crystal structures have in common that the terminal residues of the Iba proteins are not visible in the electron density. 12-16 residues of the N-terminus and 20-23 residues of the C-terminus are missing in these structures. For the Iba1 crystal structures, this observation was attributed to a partial truncation of the proteins. Furthermore, an NMR structure of h-Iba1 (PDB code 2G2B) verifies that 17 N-terminal and 18 C-terminal residues are indeed unstructured.

Iba2 is a homodimer in the crystal but not in solution

The homodimer of Iba2 observed in both crystal forms has a dimerization interface of 360 Å² corresponding to 5% of the total protein surface. This interface is unusually small for physiological homodimers because approximately 1000 Å² would be expected for a 17 kDa protein on average [23].

The Iba2 homodimer contains a central disulfide bond formed by Cys35 residues of both subunits. Considering that the crystallization of Iba2 is difficult to reproduce, the disulfide bond formation seems to occur after consumption of the reducing agent DTT by oxygen in the crystallization plates. Residue Cys35 is not conserved in Iba1. In Iba2, it appears to be conserved, but it must be noted that its gene has only been sequenced from four mammals so far.

Furthermore, the dimer in Iba2_t contains two Zn²⁺ ions bound in a symmetrical fashion inside the interface, whereas both dimers in Iba2_o coordinate only one Zn²⁺ ion each in an asymmetric geometry. This inconsistency suggests that the Zn²⁺ coordination may not appear *in vivo*, but only during crystallization in presence of 100 mM zinc acetate, where it provides essential crystal contacts. In conclusion, the homodimerization observed in both Iba2 structures seems to be restricted to the crystalline state.

It was shown previously that symmetric proteins, such as homodimers, crystallize more readily on average than asymmetric, monomeric proteins by a factor of ca. 1.5 [24]. Thus, it was suggested to dimerize monomers artificially by disulfide bonds between single cysteine residues introduced by site-directed mutagenesis [24]. In the case of Iba2, a natural cysteine residue causes the protein to dimerize. Furthermore, the Zn²⁺-coordination contacts prevent the dimer from rotating around the disulfide bond. In crystal form Iba2_t, the internal symmetry of the dimer is embodied within the crystal symmetry, such that the dimer is located with its axis of symmetry on an axis of two-fold symmetry in the crystal. Therefore, only one monomer constitutes the asymmetric unit of this crystal form. In crystal form Iba2_o, on the other hand, the crystal symmetry takes no advantage of the internal symmetry. Hence, the asymmetric unit contains 2 dimers.

Analytical ultracentrifugation showed that both human Iba proteins are able to dimerize to some extent. Nevertheless, the dimer formed in solution seems to differ from the crystallized Iba2 dimer because the ultracentrifugation experiments were conducted in presence of a reducing agent and in the absence of Zn²⁺. Thus, disulfide bond formation as well as Zn²⁺-assisted contacts were disfavored. The rather weak dissociation constants indicate that only a small fraction of the Iba proteins exists as dimers *in vivo*, although the dimerization process might be accelerated by other factors such as actin binding. The dimer in solution is probably analogous to the dimer observed in the m-Iba1 structure, where the dimeric form was obviously trapped in the crystallization process.

The function of Iba proteins does not depend on Ca²⁺

Equilibrium dialysis showed that neither Iba1 nor Iba2 bind Ca²⁺ in presence of 100 μM Ca²⁺ and ultracentrifugation revealed no significant influence of Ca²⁺ on the homodimerization. It is possible that the proteins bind calcium ions at higher concentrations than tested here. However, it should be noted that the Ca²⁺ concentration found in the cytoplasm of mammalian cells, where the native Iba proteins are localized, is 0.1–10 μM. Calcium overlays had demonstrated weak calcium binding of Iba1 EF-hand 1, but not of EF-hand 2 [3, 25], in contrast to the m-Iba1 crystal structure [4], which revealed a calcium ion bound to EF-hand 2 only.

Ca²⁺ binding had been reported to be necessary for Iba1 function in membrane ruffling and phagocytosis [3] and to enhance the interaction of Iba1 with F-actin to a certain degree [11]. In the present study F-actin binding and crosslinking by Iba proteins was calcium-independent, confirming previous results for Iba1 [12, 25]. These differing results may be due to the difficulties of quantifying actin binding exactly.

Our study indicates that neither Iba protein binds nor depends on Ca²⁺ for its function. We conclude that their actin binding and crosslinking activity has to be regulated by other factors than Ca²⁺.

EF-hand 1 is functionally inactive

Calcium ions in typical EF-hands are coordinated by six to seven oxygen atoms in pentagonal bipyramidal geometry. Classical EF-hand proteins like calmodulin and troponin C with a high Ca²⁺ affinity possess three to four acidic residues that bind the calcium ion via their negatively charged side chains [18].

EF-hand 1 was not observed to bind Ca²⁺ in any Iba structure. The conformation of the EF-hand 1 loop is very similar in all these structures: a type I β-turn, which is stabilized by several hydrogen bonds. This β-turn conformation is not observed in typical EF-hand loop structures [26]. It is very rare and has so far only been observed in the human S100 protein psoriasin (S100A7) [27]. This loop conformation prevents binding of Ca²⁺ to EF-hand 1 without prior spatial rearrangement. Although EF-hand 1 of the Iba proteins shows some resemblance with the consensus sequence, the crucial glutamate in the last position of the motif (the ‘-Z’ position) [28] is substituted mostly by serines or glycines. The coordination of Ca²⁺ by the -Z glutamate is the prime reason for the movement of the outgoing helix and the conformational change of EF-hand proteins upon Ca²⁺ binding [18]. Thus, it may be concluded that EF-hand 1 of the Iba proteins is not capable of functional Ca²⁺ binding.

Function of EF-hand 2

In both Iba1 crystal structures, the loops of EF-hand 2 adopt essentially the same conformation (Fig. 9C). In Iba2, on the other hand, residues 96–100 of the loop are in a different, more open conformation, and a rearrangement would be necessary to bind a calcium ion. A closer inspection of both Iba1 crystal structures shows that the open loop conformation was not possible because of steric clashes with adjacent molecules in their crystal lattices. The NMR structure of m-Iba1 (PDB code 2G2B) indicates that both conformations coexist in solution.

Crystal structures with bound calcium ions could neither be obtained for h-Iba1 [4] nor for Iba2. Only in m-Iba1 was Ca^{2+} observed to bind to EF-hand 2 [4]. It should be noted, however, that the Ca^{2+} concentration of 2.5 mM used for the crystallization is two orders of magnitude higher than that in the cytoplasm. This large discrepancy raises the question if the observed Ca^{2+} binding can occur *in vivo*.

In contrast to classical EF-hand proteins, the Ca^{2+} in m-Iba1 is not coordinated in pentagonal bipyramid geometry, but resides in the center of a distorted tetrahedron. There are additional contributions by the Thr100 carbonyl group at an unusual angle and a water molecule. A comparison of EF-hand 2 with the consensus motif [26] shows that it does not contain any acidic residues for the Ca^{2+} coordination in the N-terminal half (Fig. 1). However, this first half of the loop is supposed to bind the calcium ion initially [18]. Furthermore, the last residue of the loop, the $-Z$ position, is not a glutamate but a shorter aspartate residue, which cannot bind Ca^{2+} in a bidentate manner as glutamate usually does. Overall, the Ca^{2+} coordination appears too weak to overcome the energy barrier of the conformational rearrangement giving rise to the dimerization observed in the m-Iba1 structure. Moreover, the conformational change from the monomeric Iba structures to the dimeric m-Iba1 is very different from that of any known EF-hand protein. Surprisingly, it is not the outgoing helix αD of EF-hand 2, which shifts its location, but the incoming helix αC . Furthermore, there is a more pronounced rearrangement in EF-hand 1 than in EF-hand 2, although EF-hand 1 does not bind Ca^{2+} . Therefore, it may be questioned if the rearrangement and dimerization of the Iba proteins are indeed caused by Ca^{2+} binding.

Cellular localization and recruitment to sites of *Shigella* invasion

While intracellular localization patterns of Iba2 were similar to patterns seen with Iba1 constructs, Iba2 recruitment into peripheral structures was less pronounced, resulting in a less distinct peripheral pattern compared with Iba1 (Fig. 7, 8). We used a model for *Shigella*

invasion of epithelial cells [22] to study Iba recruitment into bacteria-induced membrane ruffles. In this model, Rac and RhoA are recruited around entering bacteria (peribacterial recruitment), while RhoC and the ERM protein ezrin accumulate in cellular protrusions [29]. Peribacterial protein recruitment is considered to be part of early invasion steps; whereas protein recruitment into membrane ruffles occurs at a later stage of infection [29]. In the present study, no peribacterial recruitment of the Iba proteins was observed. In the *Shigella* invasion model of epithelial cells, CDC42, Rac and Rho are essential for efficient internalization of the bacteria [30-32]. Interestingly, Iba1 has been associated with Rac-mediated membrane ruffling in a variety of cells. However, direct protein-protein interaction of Rac and Iba1 has not been reported [3, 33, 34]. Thus, our finding of *Shigella*-induced Iba recruitment into membrane ruffles in contrast to the peribacterial staining pattern of Rac is compatible with the view that Iba and Rac proteins do not directly interact with each other during *Shigella* invasion of epithelial cells. The peripheral staining pattern seen in the bacterial invasion model suggests a role for Iba downstream of Rac activation. This is in agreement with data showing inhibition by an Iba deletion mutant of cellular protrusions induced by constitutively active Rac [3]. A potential role for the Iba proteins in generation and/or maintenance of *Shigella*-induced membrane ruffles is stabilizing membrane-associated actin filaments by crosslinking, similar to Iba activity in phagocytes [12]. In addition to Iba, the actin crosslinking proteins α -actinin [32] and plastin [22] have been found in *Shigella* entry sites, showing recruitment patterns similar to Iba. While the morphology of Iba-induced actin bundles has been described [12], it is unknown whether Iba-mediated bundling of F-actin is sensitive to the orientation of actin filaments. Similarly, nothing is known about potentially functional differences between Iba isoforms due to the slightly varying recruitment patterns described here.

Conserved surface residues and actin crosslinking

In sequence alignments, highly conserved regions of the Iba proteins become apparent (Fig. 1). When the conservation of residues is plotted on the protein surface, Iba1 and Iba2 show very similar highly conserved regions (Fig. 10A-B). As expected, the residues comprising the Iba1 dimerization interface are highly conserved in Iba1 as well as in Iba2. Surprisingly, the helix-loop-helix region α B- α C, which comprises the outgoing helix of EF-hand 1 and the incoming helix of EF-hand 2, is also strictly conserved; even though it is solvent-exposed. This region contains several hydrophobic residues on the surface and is almost uncharged, while it is surrounded by highly charged patches (Fig. 10C). This helix-loop-helix region

undergoes a structural rearrangement upon dimerization in m-Iba1 [4] and was observed to be flexible in one of the four molecules in Iba2_o. Thus, this conserved region may constitute an interface for interaction with another protein, possibly actin.

It is likely that Iba monomers, due to their small size, have only one F-actin binding site. Consequently, F-actin crosslinking would require Iba homodimerisation. We observed Iba homodimerisation in our analytical ultracentrifugation experiments and the crystal structure of mIba1 [4] shows a homodimer. The role of Iba homodimerisation in F-actin crosslinking remains to be studied.

Conclusion

According to our studies, Iba1 and Iba2 share similar overall structures and molecular functions. They are able to crosslink actin, which probably requires dimerization of the Iba proteins. The actin-crosslinking ability might play a role during the invasion of host cells by *Shigella* and other invasive pathogens. While Iba2 generally appears to be less active than Iba1, the most outstanding difference between both Iba proteins seems to be their distinct expression patterns in various tissues of the body.

Experimental procedures

Cloning

A full-length human Iba2 cDNA fragment (GenBank CAB66501) was amplified by PCR from the clone DKFZp761J191 [15]. Primers CTG GAT CCT CGG GCG AGC TCA GCA AC and GAC GGC GGC CGC TCA GGG CAG GCT AGC AAT GTC T were used. The PCR product was cloned into the vector pQTEV (GenBank AY243506) using BamHI and NotI restriction sites and introduced into *E. coli* SCS1 cells carrying the pRARE plasmid [35], and a resulting clone was used for overexpression of Iba2 (GenBank DQ000573, PSF ID 109968, RZPD ID PSFEp250B085).

cDNA clones of the LIFEdb [16] for expression of human Iba2 as C-terminal YFP or N-terminal CFP fusion proteins were a gift from Stephanie Bechtel and Stefan Wiemann (DKFZ Heidelberg). These plasmids contain the DKFZp761J191 open reading frame in the vectors pdEYFP-N1gen and pdECFP-C1amp, respectively [17].

The open reading frame of the human Iba1 cDNA clone IOH13810 (Invitrogen), corresponding to GenBank NM_001623, was obtained from the RZPD German Resource Center in the expression vector pDEST17-D18. BL21(DE3) *E. coli* cells were transformed for protein expression. The same cDNA was also obtained in the vectors pdEYFP-C1amp and pdEYFP-N1gen [17] for expression of C-terminal and N-terminal YFP fusion proteins in mammalian cells.

Fermentation and purification

Iba2 was prepared for crystallization as follows. Clone ID 109968 was fermenter-grown to an OD₆₀₀ of 8 in 4 L of SB medium (12 g/L bacto-tryptone, 24 g/L yeast extract, 0.4% (v/v) glycerol, 17 mM KH₂PO₄, 72 mM K₂HPO₄) supplemented with 20 µg/mL thiamine, 100 µg/mL ampicillin and 34 µg/mL chloramphenicol. Protein expression was induced with 1 mM isopropyl-β-D-thiogalactopyranoside (IPTG) for 3 h at 37 °C. Cells were pelleted by centrifugation and washed with extraction buffer (20 mM Tris-HCl, pH 8.0, 300 mM NaCl, 0.5 mM EDTA (ethylenediaminetetraacetic acid), 1 mM PMSF (phenylmethylsulfonyl-fluoride), 5 mM 2-mercaptoethanol). The cells were lysed, and cell lysates and proteins were stored at 4 °C. Protein purification steps were performed at room temperature. The pellets of the protein-expressing cells were resuspended in a 4-fold volume of extraction buffer. Lysozyme was added to 0.4 mg/mL and cells were disrupted by sonification. Cellular debris was removed by centrifugation (55,000×g, 45 min), and the supernatant was filtrated through cellulose nitrate (0.45 µm). The pH of the solution was adjusted to pH 7.4 and the extract was applied to a 10-mL TALON Superflow 16/20 column (BD Biosciences) equilibrated with buffer (20 mM Tris-HCl, pH 7.4, 500 mM NaCl, 10 mM imidazole). The protein was eluted using buffer containing 50 mM NaCl, 200 mM imidazole, 0.5 mM EDTA, and 1 mM DTT (dithiothreitol). TEV protease (1:40) was added to remove the His₆ tag (2 h, 4 °C). The protein solution was diluted 5-fold in 20 mM Tris-HCl, pH 7.4 and applied to a 8-mL POROS 20 S cation-exchange chromatography column (Applied Biosystems), mainly to remove the TEV protease. The flow-through of the cation-exchange chromatography was applied to a POROS 20 HQ anion-exchange chromatography column (4 mL volume), and Iba2 was again found in the flow-through. After size-exclusion chromatography (Superdex 75 XK 16/60, Amersham) the protein yield was 177 mg. Samples were concentrated using Vivaspin 10 concentrators (Vivascience) and stored in 15 mM Tris-HCl, pH 7.4, 50 mM NaCl, 0.1 mM EDTA, 2 mM DTT, 0.02% NaN₃.

Iba1 and Iba2 for binding studies were prepared as described above, but without ion exchange chromatography. The N-terminal His₆ tag of the Iba1 protein product (19kDa) was not removed, while Iba2 was used without tag (17 kDa). The purified and concentrated proteins were shown to be monodisperse by dynamic light scattering (Laser Scatter201, RiNA GmbH, Germany).

Crystallization

Iba2 was crystallized by the sitting-drop vapour-diffusion method at 20 °C. 400 µL of protein (18.1 mg/mL in 15 mM Tris-HCl, pH 7.4, 50 mM NaCl, 0.02% NaN₃, 2 mM DTT and 0.1 mM EDTA) were added to 400 µL of reservoir solution (13-15% [w/v] PEG 4000, 100 mM Na-acetate, pH 5.0, and 100 mM zinc acetate). Crystals of two distinct morphologies grew within two weeks: an orthorhombic crystal form (Iba2_o) with a size of 1000 × 300 × 50 µm and trigonal crystals (Iba2_t) with sizes of 500 × 400 × 400 µm. Prior to X-ray data collection, 20% (v/v) PEG 400 was added for cryo-protection. Iba2_t crystals belong to space group P3₂21 with cell constants $a=b=70.5$ and $c=95.2$ Å. These crystals contain one Iba2 molecule per asymmetric unit with a V_M -value [36] of 4.0 Å³/Da and a solvent content of 69%. Iba2_o crystals belong to space group P2₁2₁2 with cell constants $a=71.5$, $b=186.5$ and $c=51.4$ Å. A V_M -value of 2.5 Å³/Da corresponding to a solvent content of 51% was obtained for a lattice with four molecules in the asymmetric unit.

Data collection, structure determination and analysis

X-ray diffraction data were collected at the BESSY beamline BL14.1 [37]. Data were processed with XDS [38] and scaled with Scala of the CCP4 program suite [39]. The structure of m-Iba1 [4] (PDB code 1WY9) served as a model for molecular replacement using Phaser [40]. CNS [41] was used for rigid-body and simulated-annealing refinement, REFMAC [42] for subsequent refinement, including TLS protocols. Coot was used for manual model building and structural analysis [43]. The structures were validated using WHAT IF [44] and PROCHECK [45]. Molecular drawings were prepared using PyMOL [46]. LSQKAB of the CCP4 suite [39] was used to calculate root-mean-square deviations and DALI [47] to identify structural protein homologs.

Purification of actin

Non-muscle β-actin was purified from bovine brain [48, 49]. Briefly, the method involved affinity purification of profilin-actin complexes on poly-L-proline Sepharose, enrichment of

actin by a cycle of polymerization and depolymerization, isoform separation by hydroxyapatite chromatography, and a final gel filtration step.

Actin cosedimentation and crosslinking assays

Samples of actin (4 μM) were induced to polymerize by addition of 1 mM MgCl_2 and 0.15 M KCl alone or in the presence of Iba1 or Iba2, and incubated at room temperature for 2-3 h. Dependency on Ca^{2+} was assessed using either 0.5 mM CaCl_2 or 0.5 mM EGTA in the polymerization buffer. For cosedimentation analyses, samples were subjected to ultracentrifugation at $200,000\times g$ for 45 min at 22 °C in a Beckman Maxima. For crosslinking analyses, samples were centrifuged at $8000\times g$ in a tabletop centrifuge. In each case, equal amounts of the supernatants and pellets were analyzed by SDS-PAGE and Coomassie staining.

In vitro actin fluorescence microscopy

Actin polymers (4 μM) formed under the above conditions were supplemented with 100 nM Alexa488-phalloidin (Invitrogen) and incubated at room temperature on cover slips alone or in the presence of Iba1 or Iba2 (0.5 μM), or neurabin-2 with an intact or truncated actin binding domain (1 μM) [50]. Samples were mounted in Vectashield (Vector Laboratories) and imaged using a 100x Fluoroplan oil immersion lens on a Zeiss Axioplan-2 microscope, and images were captured using a Zeiss AxioCam camera and AxioVision imaging software.

Calcium equilibrium dialysis

Equilibrium dialysis was performed according to Stevens *et al.* [51]. The buffer of purified Iba1 and Iba2 was exchanged against ED buffer (20 mM PIPES-NaOH, pH 7.0, 100 mM NaCl, 1 mM DTT) by dialysis. Calmodulin from bovine brain (Sigma) was dissolved in ED buffer. 160 μM Iba1, 160 μM Iba2 and 40 μM calmodulin were used, because calmodulin contains four Ca^{2+} binding sites. Equilibrium dialysis was performed for 20 h at room temperature in 3.5K Slide-A-Lyzer Dialysis Cassettes (Pierce) against 250 mL ED buffer containing 100 μM CaCl_2 and 7 kBq/mL $^{45}\text{CaCl}_2$. 50 μL aliquots of the dialysis buffer and protein samples were measured in a scintillation counter. Protein integrity was verified by dynamic light scattering and SDS-PAGE before and after the dialysis.

Disulfide-bond formation assay

Purified Iba2 in 20 mM Tris-HCl, pH 7.5, 100 mM NaCl, 0.1 mM EDTA was incubated for one week at 10 °C alone or in the presence of either 2.5 mM CaCl₂, 2 mM DTT or both. Proteins were analyzed by non-reducing SDS-PAGE and Coomassie staining.

Quaternary structure determination by analytical ultracentrifugation

Molecular mass studies on the human Iba proteins were performed using an analytical ultracentrifuge (Beckman XL-A, Palo Alto, USA) equipped with absorbance optics. Samples of about 70 µL protein with increasing concentrations were centrifuged 2 h at 26,000 rpm, 10 °C (over-speed) in externally loaded six-channel cells against buffer (20 mM Tris-HCl, pH 7.5, 100 mM NaCl, 0.1 mM EDTA, TCEP) alone or in the presence of 2.5 mM CaCl₂. Sedimentation equilibrium was reached by a subsequent 26–30 h run at 10 °C. The radial concentration distributions of each sample were recorded at three different wavelengths between 260 and 290 nm and fitted globally to Eq. (1):

$$A_r = A_{rm} \cdot e^{MK} \quad \text{with} \quad K = \frac{(1 - \rho \bar{v}) \omega^2 (r^2 - r_m^2)}{2RT} \quad (1)$$

using POLYMOLE [52]. In these equations, ρ is the solvent density, \bar{v} is the partial specific volume of the Iba protein, ω is the angular velocity, R is the gas constant and T the absolute temperature. A_r is the radial absorbance and A_{rm} represents the corresponding value at the meniscus position. When proteins adopt a monomer-dimer equilibrium, the molecular mass, M , can be treated as a weight average parameter (M_w).

In the present case, this value is a composite of the molecular mass values M_m and M_d and the partial concentrations of monomers, c_m , and dimers, c_d , according to Eq. (2)

$$M_w = \frac{c_m \cdot M_m + c_d \cdot M_d}{c_m + c_d} \quad (2)$$

Therefore, the equilibrium constant can be determined with $K_d = c_m^2 / c_d$ (3)

Culture and transfection of HeLa cells

HeLa cells were grown on 22 × 22 mm cover slips placed in 6-well plates with 2 mL of minimal essential medium (MEM with Earle's salts and glutamine) with 10% fetal calf serum (FCS). Standard calcium phosphate precipitation techniques [53] with 6 µg of plasmid DNA per well of a 6-well plate were employed for transient transfection of HeLa cells 24 h prior to bacterial infection.

***Shigella* strains**

SC301 is derived from the wild-type invasive strain M90T, SC300 is derived from BS176, a non-invasive mutant of M90T cured of the large virulence plasmid. *Shigella* strains SC300 and SC301 contain plasmid pIL22 encoding an afimbrial adhesin of uropathogenic *E. coli* [54].

***Shigella* infection of HeLa cells**

Infection of HeLa cells was performed as described previously [29]. Briefly, bacteria were grown to mid-exponential phase in tryptic soy broth (TSB), centrifuged, PBS-washed and resuspended in MEM. Cells were washed twice with MEM and the medium replaced by 2 mL of the bacterial suspension (6×10^7 /mL) at room temperature (rt). After sedimentation of the bacteria at rt, the preparation was set on top of a water bath at 37 °C to trigger the infection. After 13 min of infection, preparations were washed 5 times with PBS and fixed in 3.7% (w/v) formaldehyde in PBS.

Immunofluorescence techniques

Formaldehyde-fixed preparations were quenched with 100 mM glycine in phosphate buffered saline (PBS) for 5 min. Bacteria were stained with DAPI (5 μ M in PBS, Molecular Probes). F-actin was labelled with Alexa594-phalloidine (1/40, Molecular Probes). The preparations were studied with an inverted fluorescence microscope (Axiovert 135, Carl Zeiss) equipped with a position servo controller (E-662, Physik Instrumente) for registration of 20 parallel focus planes. Distance between planes was 0.3 mm. Pictures were taken with a Spot PursuitTM monochrome camera (Diagnostic Instruments). Image stacks were processed using AutodeblurTM (Media Cybernetics) deconvolution software.

Accession number

The coordinates of both structures have been deposited in the RCSB Protein Data Bank (PDB codes 2vtg and 2jjz).

Acknowledgements

We wish to thank Nabila Ibrahim, Anja Koch, Thomas Grund, Dinh-Trung Pham and Janett Tischer for technical assistance and Ulrich Harttig for help in target selection. This work was funded by the German Federal Ministry for Education and Research (BMBF) through the "Leitprojektverbund Proteinstrukturfabrik", the National Genome Network (NGFN; FZK 01GR0471, 01GR0472) and with support by the Fonds der Chemischen Industrie to U.H.

References

1. Imai Y, Iбата I, Ito D, Ohsawa K & Kohsaka S (1996) A novel gene *iba1* in the major histocompatibility complex class III region encoding an EF hand protein expressed in a monocytic lineage. *Biochemical and Biophysical Research Communications* **224**, 855-862.
2. Kawasaki H, Nakayama S & Kretsinger RH (1998) Classification and evolution of EF-hand proteins. *Biometals* **11**, 277-295.
3. Ohsawa K, Imai Y, Kanazawa H, Sasaki Y & Kohsaka S (2000) Involvement of *Iba1* in membrane ruffling and phagocytosis of macrophages/microglia. *Journal of cell science* **113**, 3073-3084.
4. Yamada M, Ohsawa K, Imai Y, Kohsaka S & Kamitori S (2006) X-ray structures of the microglia/macrophage-specific protein *Iba1* from human and mouse demonstrate novel molecular conformation change induced by calcium binding. *Journal of Molecular Biology* **364**, 449-457.
5. Shyamsundar R, Kim YH, Higgins JP, Montgomery K, Jorden M, Sethuraman A, van de Rijn M, Botstein D, Brown PO & Pollack JR (2005) A DNA microarray survey of gene expression in normal human tissues. *Genome biology* **6**, R22.
6. Autieri MV (1996) cDNA cloning of human allograft inflammatory factor-1: tissue distribution, cytokine induction, and mRNA expression in injured rat carotid arteries. *Biochemical and Biophysical Research Communications* **228**, 29-37.
7. Utans U, Arceci RJ, Yamashita Y & Russell ME (1995) Cloning and characterization of allograft inflammatory factor-1: a novel macrophage factor identified in rat cardiac allografts with chronic rejection. *The Journal of clinical investigation* **95**, 2954-2962.
8. Utans U, Quist WC, McManus BM, Wilson JE, Arceci RJ, Wallace AF & Russell ME (1996) Allograft inflammatory factor-1. A cytokine-responsive macrophage molecule expressed in transplanted human hearts. *Transplantation* **61**, 1387-1392.
9. Autieri MV, Carbone C & Mu A (2000) Expression of allograft inflammatory factor-1 is a marker of activated human vascular smooth muscle cells and arterial injury. *Arteriosclerosis, Thrombosis, and Vascular Biology* **20**, 1737-1744.
10. Köhler C (2007) Allograft inflammatory factor-1/Ionized calcium-binding adapter molecule 1 is specifically expressed by most subpopulations of macrophages and spermatids in testis. *Cell Tissue Res* **330**, 291-302.
11. Autieri MV, Kelemen SE & Wendt KW (2003) AIF-1 is an actin-polymerizing and Rac1-activating protein that promotes vascular smooth muscle cell migration. *Circulation Research* **92**, 1107-1114.
12. Sasaki Y, Ohsawa K, Kanazawa H, Kohsaka S & Imai Y (2001) *Iba1* is an actin-cross-linking protein in macrophages/microglia. *Biochemical and Biophysical Research Communications* **286**, 292-297.

13. Ohsawa K, Imai Y, Sasaki Y & Kohsaka S (2004) Microglia/macrophage-specific protein Iba1 binds to fimbrin and enhances its actin-bundling activity. *Journal of Neurochemistry* **88**, 844-856.
14. Büssow K, Scheich C, Sievert V, Harttig U, Schultz J, Simon B, Bork P, Lehrach H & Heinemann U (2005) Structural Genomics of human proteins - target selection and generation of a public catalog of expression clones. *Microbial Cell Factories* **4**, 21.
15. Wiemann S, Weil B, Wellenreuther R, Gassenhuber J, Glassl S, Ansorge W, Böcher M, Blöcker H, Bauersachs S, Blum H, Lauber J, Dusterhöft A, Beyer A, Köhrer K, Strack N, Mewes HW, Ottenwälder B, Obermaier B, Tampe J, Heubner D, Wambutt R, Korn B, Klein M & Poustka A (2001) Toward a catalog of human genes and proteins: sequencing and analysis of 500 novel complete protein coding human cDNAs. *Genome Research* **11**, 422-435.
16. Bannasch D, Mehrle A, Glatting KH, Pepperkok R, Poustka A & Wiemann S (2004) LIFEdb: a database for functional genomics experiments integrating information from external sources, and serving as a sample tracking system. *Nucleic Acids Research* **32**, D505-D508.
17. Simpson JC, Wellenreuther R, Poustka A, Pepperkok R & Wiemann S (2000) Systematic subcellular localization of novel proteins identified by large-scale cDNA sequencing. *EMBO reports* **1**, 287-292.
18. Grabarek Z (2006) Structural basis for diversity of the EF-hand calcium-binding proteins. *Journal of Molecular Biology* **359**, 509-525.
19. Chattopadhyaya R, Meador WE, Means AR & Quijcho FA (1992) Calmodulin structure refined at 1.7 Å resolution. *Journal of Molecular Biology* **228**, 1177-1192.
20. Rao ST, Satyshur KA, Greaser ML & Sundaralingam M (1996) X-ray structures of Mn, Cd and Tb metal complexes of troponin C. *Acta Crystallographica Section D-Biological Crystallography* **52**, 916-922.
21. Tang JX & Janmey PA (1998) Two distinct mechanisms of actin bundle formation. *The Biological bulletin* **194**, 406-408.
22. Adam T, Arpin M, Prevost MC, Gounon P & Sansonetti pj (1995) Cytoskeletal rearrangements and the functional role of T-plastin during entry of *Shigella flexneri* into HeLa cells. *Journal of Cell Biology* **129**, 367-381.
23. Jones S & Thornton JM (1996) Principles of protein-protein interactions. *Proc Natl Acad Sci USA* **93**, 13-20.
24. Banatao DR, Cascio D, Crowley CS, Fleissner MR, Tienson HL & Yeates TO (2006) An approach to crystallizing proteins by synthetic symmetrization. *Proc Natl Acad Sci USA* **103**, 16230-16235.
25. Autieri MV & Chen X (2005) The ability of AIF-1 to activate human vascular smooth muscle cells is lost by mutations in the EF-hand calcium-binding region. *Exp Cell Res* **307**, 204-211.
26. Gifford JL, Walsh MP & Vogel HJ (2007) Structures and metal-ion-binding properties of the Ca²⁺-binding helix-loop-helix EF-hand motifs. *The Biochemical Journal* **405**, 199-221.

27. Brodersen DE, Etzerodt M, Madsen P, Celis JE, Thøgersen HC, Nyborg J & Kjeldgaard M (1998) EF-hands at atomic resolution: the structure of human psoriasin (S100A7) solved by MAD phasing. *Structure* **6**, 477-489.
28. Lewit-Bentley A & Rety S (2000) EF-hand calcium-binding proteins. *Curr Opin Struct Biol* **10**, 637-643.
29. Graf B, Bähler M, Hilpelä P, Böwe C & Adam T (2000) Functional role for the class IX myosin myr5 in epithelial cell infection by *Shigella flexneri*. *Cellular microbiology* **2**, 601-616.
30. Adam T, Giry M, Boquet P & Sansonetti P (1996) Rho-dependent membrane folding causes *Shigella* entry into epithelial cells. *The EMBO journal* **15**, 3315-3321.
31. Mounier J, Laurent V, Hall A, Fort P, Carlier MF, Sansonetti PJ & Egile C (1999) Rho family GTPases control entry of *Shigella flexneri* into epithelial cells but not intracellular motility. *Journal of cell science* **112**, 2069-2080.
32. Tran Van Nhieu G, Caron E, Hall A & Sansonetti PJ (1999) IpaC induces actin polymerization and filopodia formation during *Shigella* entry into epithelial cells. *The EMBO journal* **18**, 3249-3262.
33. Kanazawa H, Ohsawa K, Sasaki Y, Kohsaka S & Imai Y (2002) Macrophage/microglia-specific protein Iba1 enhances membrane ruffling and Rac activation via phospholipase C-gamma -dependent pathway. *The Journal of biological chemistry* **277**, 20026-20032.
34. Tian Y & Autieri MV (2007) Cytokine expression and AIF-1-mediated activation of Rac2 in vascular smooth muscle cells: a role for Rac2 in VSMC activation. *American journal of physiology* **292**, C841-849.
35. Novy R, Drott D, Yaeger K & Mierendorf R (2001) Overcoming the codon bias of *E.coli* for enhanced protein expression. *inNovations* **12**, 1-3.
36. Matthews BW (1968) Solvent content of protein crystals. *Journal of Molecular Biology* **33**, 491-497.
37. Heinemann U, Büsow K, Mueller U & Umbach P (2003) Facilities and methods for the high-throughput crystal structural analysis of human proteins. *Acc Chem Res* **36**, 157-163.
38. Kabsch W (1993) Automatic processing of rotation diffraction data from crystals of initially unknown symmetry and cell constants. *Journal of Applied Crystallography* **26**, 795-800.
39. Collaborative Computational Project N (1994) The CCP4 suite: programs for protein crystallography. *Acta Crystallographica Section D-Biological Crystallography* **50**, 760-763.
40. McCoy AJ, Grosse-Kunstleve RW, Storoni LC & Read RJ (2005) Likelihood-enhanced fast translation functions. *Acta Crystallographica Section D-Biological Crystallography* **61**, 458-464.
41. Brünger AT, Adams PD, Clore GM, DeLano WL, Gros P, Grosse-Kunstleve RW, Jiang JS, Kuszewski J, Nilges M, Pannu NS, Read RJ, Rice LM, Simonson T & Warren GL (1998) Crystallography & NMR system: A new

- software suite for macromolecular structure determination. *Acta Crystallographica Section D-Biological Crystallography* **54**, 905-921.
42. Murshudov GN, Vagin AA & Dodson EJ (1997) Refinement of macromolecular structures by the maximum-likelihood method. *Acta Crystallographica Section D-Biological Crystallography* **53**, 240-255.
43. Emsley P & Cowtan K (2004) Coot: model-building tools for molecular graphics. *Acta Crystallographica Section D-Biological Crystallography* **60**, 2126-2132.
44. Vriend G (1990) WHAT IF: a molecular modeling and drug design program. *Journal of Molecular Graphics* **8**, 52-56, 29.
45. Laskowski RA, MacArthur MW, Moss DS & Thornton JM (1993) PROCHECK: a program to check the stereochemical quality of protein structures. *Journal of Applied Crystallography* **26**, 283-291.
46. DeLano WL (2002) *The PyMOL User's Manual* DeLano Scientific, San Carlos, CA, USA.
47. Holm L & Sander C (1996) Mapping the protein universe. *Science* **273**, 595-603.
48. Lindberg U, Schutt CE, Hellsten E, Tjader AC & Hult T (1988) The use of poly(L-proline)-Sepharose in the isolation of profilin and profilactin complexes. *Biochimica et biophysica acta* **967**, 391-400.
49. Schüler H, Karlsson R & Lindberg U (2005) Purification of non-muscle actin. In *Cell Biology: A Laboratory Handbook* (Celis J, ed^s). Academic Press, New York.
50. Schüler H & Peti W (2008) Structure-function analysis of the filamentous actin binding domain of the neuronal scaffolding protein spinophilin. *FEBS Journal* **275**, 59-68.
51. Stevens J & Rogers JH (1997) Chick calretinin: purification, composition, and metal binding activity of native and recombinant forms. *Protein expression and purification* **9**, 171-181.
52. Behlke J, Ristau O & Schönfeld HJ (1997) Nucleotide-dependent complex formation between the Escherichia coli chaperonins GroEL and GroES studied under equilibrium conditions. *Biochemistry* **36**, 5149-5156.
53. Sambrook J, Fritsch EF & Maniatis T (1989) *Molecular Cloning: a laboratory manual*, 2 edn. Cold Spring Harbor Laboratory.
54. Clerc P & Sansonetti PJ (1987) Entry of Shigella flexneri into HeLa cells: evidence for directed phagocytosis involving actin polymerization and myosin accumulation. *Infection and Immunity* **55**, 2681-2688.

Figure Legends

Fig. 1. Sequence alignment of human Iba1 [4] and Iba2. Identical residues are shown in black, non-identical residues in gray. Assigned secondary structure elements are depicted in green for Iba1 and in blue for Iba2. The terminal regions of both proteins are not resolved. The EF-hand motifs are framed in red; a consensus EF-hand [26] is shown for comparison. The residues involved in Ca^{2+} binding are highlighted in orange.

Fig. 2. Cartoon representation of the homodimer in crystal form Iba2_t. One subunit of the dimer is rendered in gray, the other subunit is shown in blue with a transparent surface. Important residues in the dimerization interface are depicted in stick representation with oxygen atoms in red and sulfur atoms in yellow. The figures were produced using PyMOL [46].

Fig. 3. Homodimerization of Iba1 and Iba2. The molecular mass of Iba proteins against protein concentration was determined by analytical ultracentrifugation in the presence or absence of calcium ions.

Fig. 4. F-actin co-sedimentation and crosslinking. (A) Increasing amounts of Iba1 and Iba2 (0-4 μM) were incubated with 4 μM F-actin in the presence of Ca^{2+} or EGTA. Proteins were sedimented by ultracentrifugation and pellets analyzed by SDS-PAGE and Coomassie staining. (B) F-actin alone or mixed with Iba1 or Iba2 was subjected to low-speed centrifugation (8,000 $\times g$). SDS-PAGE of pellets (p) and supernatants (s) shows that F-actin sediments readily in the presence of Iba1 and Iba2.

Fig. 5. Fluorescence microscopy of actin crosslinked by Iba1 and Iba2. (A) Actin polymers stained with a fluorescent phalloidin analog. (B-C) Actin polymers in presence of Iba1 (B) and Iba2 (C). (D-E) For comparison, actin polymers are shown in the presence of the actin crosslinking protein neurabin-2 (D) and an actin binding deficient truncation mutant of neurabin-2 (E).

Fig. 6. Calcium-binding assay for Iba1 and Iba2. Iba1, Iba2 and calmodulin were dialyzed against 100 μM CaCl_2 and a trace amount of $^{45}\text{CaCl}_2$. Upon dialysis, an increased Ca^{2+} concentration was found in the calmodulin sample.

Fig. 7. Iba proteins colocalize with F-actin in HeLa cells. HeLa cells were transfected with YFP-tagged human Iba1 (B) or CFP-tagged Iba2 (E). F-actin was stained using Alexa594-phalloidine (C, F). Overlay images (A, D) show colocalization of Iba1 and Iba2 with subcortical F-actin. Iba2 is recruited to a lesser extent into cellular projections and adhesion structures than Iba1.

Fig. 8. Iba2 (A-D) and Iba1 (E-H) are recruited into *Shigella* entry zones in an invasion assay. Iba2 is less concentrated in the cell periphery. HeLa cells, transiently transfected with CFP-Iba2 (C, L) or YFP-Iba1 (F, K), were infected with *Shigella* that were visualized as small rods by DAPI DNA staining (D, H). F-actin was stained with Alexa594-phalloidine (B,G). Overlay images (A, E) show more pronounced staining of membrane ruffle-like protrusions with Iba1. Double-transfected and infected cells confirm more pronounced recruitment into cellular protrusions of Iba1 (K) compared with Iba2 (L); overlay: I

Fig. 9. Superposition of Iba2 (blue) on (A) Ca²⁺-free h-Iba1 (dark green) [4] and on (B) Ca²⁺-bound, dimeric m-Iba1 (light green) [4]. The second subunit of the m-Iba1 dimer is depicted in gray and calcium ions are shown as orange spheres. The relocation of helix αE , which is crucial for dimerization, is indicated by a black arrow. (C) Detailed view of EF-hand 2. The residues involved in Ca²⁺ coordination of m-Iba1 are shown in stick representation.

Fig. 10. Conservation of surface residues illustrated on the m-Iba1 dimer [4] depicted in (A) cartoon and (B) surface representation (the molecule is rotated by 180° in comparison to Fig. 9). Considered are Iba1 sequences from 13 species (*Homo sapiens*, *Macaca mulatta*, *Mus musculus*, *Rattus norvegicus*, *Sus scrofa*, *Bos taurus*, *Ornithorhynchus anatinus*, *Suberites domuncula*, *Haliotis discus hannai*, *Cyprinus carpio*, *Fugu rubripes*, *Pagrus major* and *Epinephelus awoara*) and Iba2 sequences from four species (*Homo sapiens*, *Pongo pygmaeus*, *Bos taurus* and *Mus musculus*). Identical residues are colored in dark blue, moderately conserved residues in green and non-conserved residues in red. (C) Electrostatic potential on the surface of the m-Iba1 dimer.

Figure 1

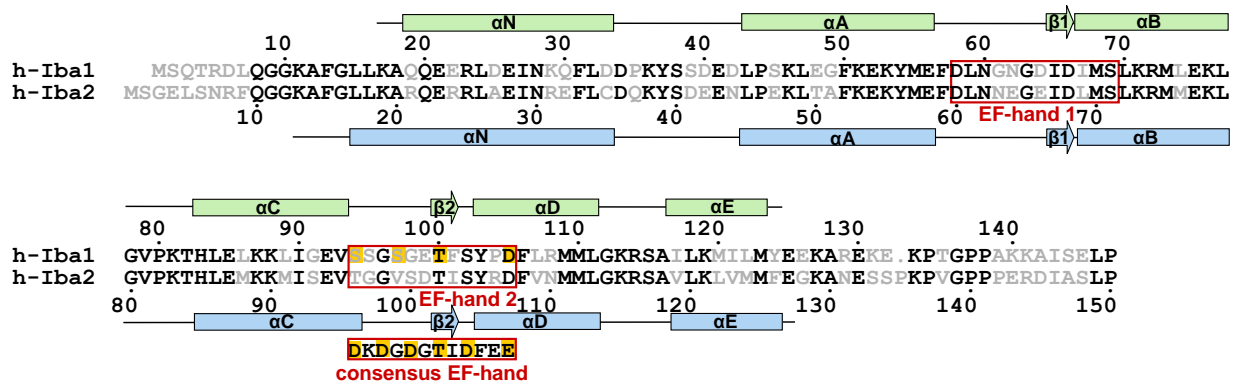


Figure 2

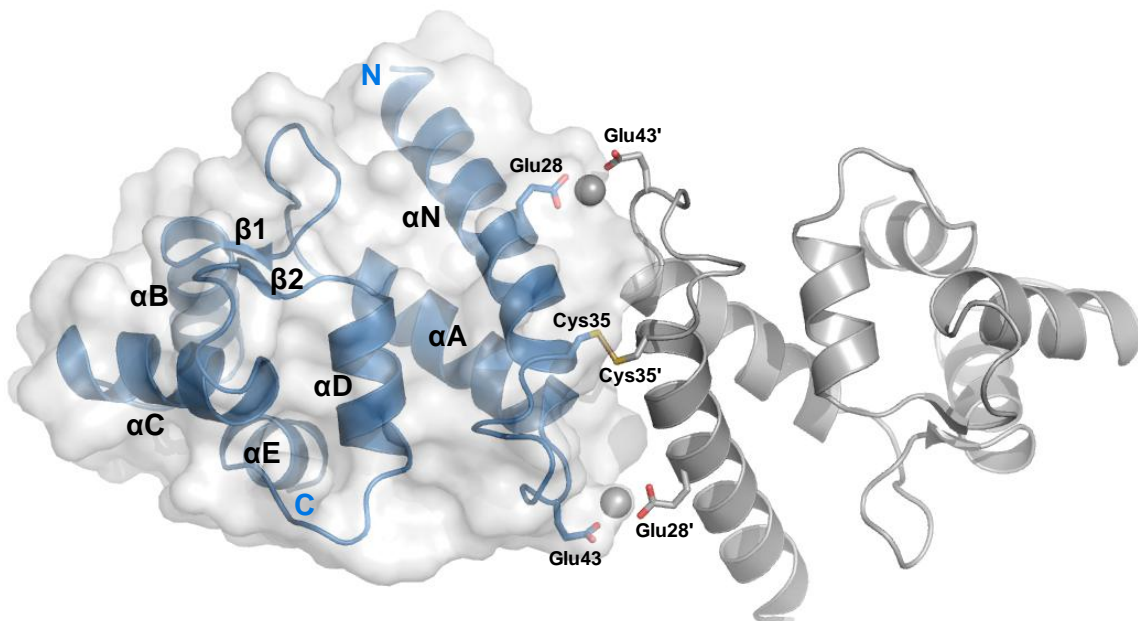


Figure 3

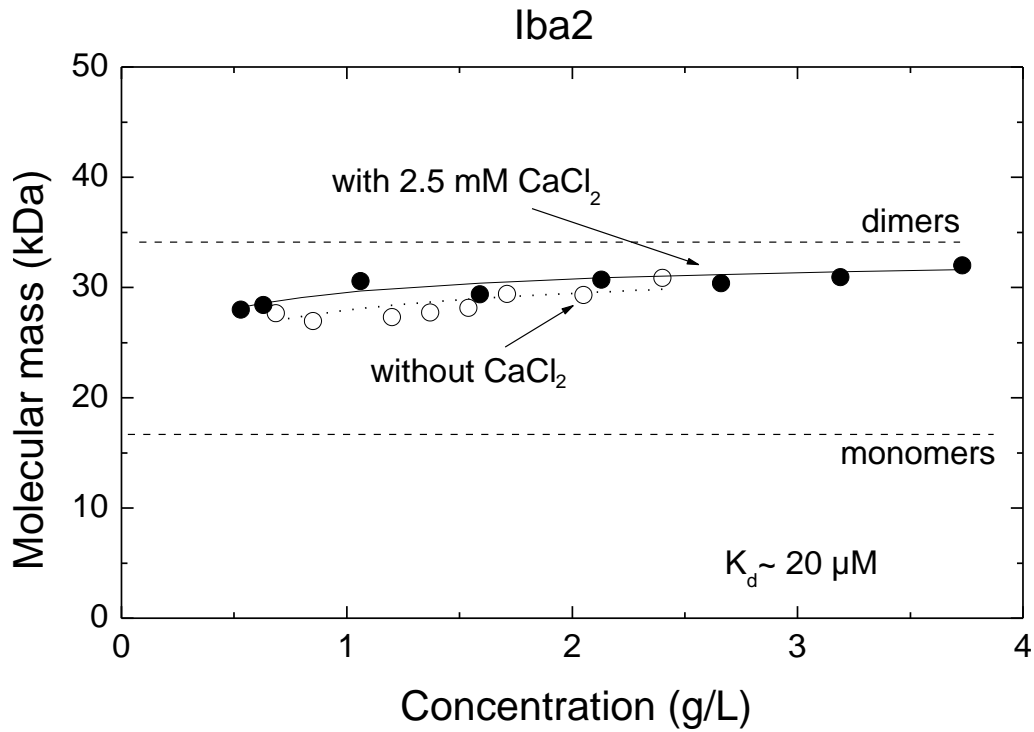
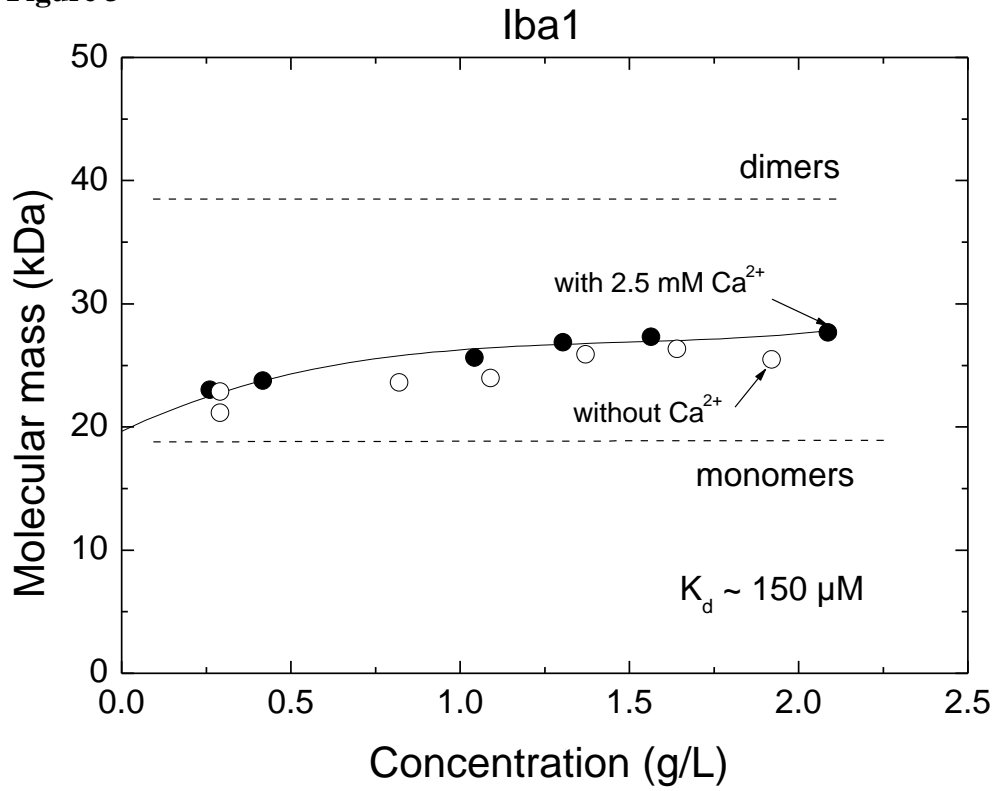


Figure 4

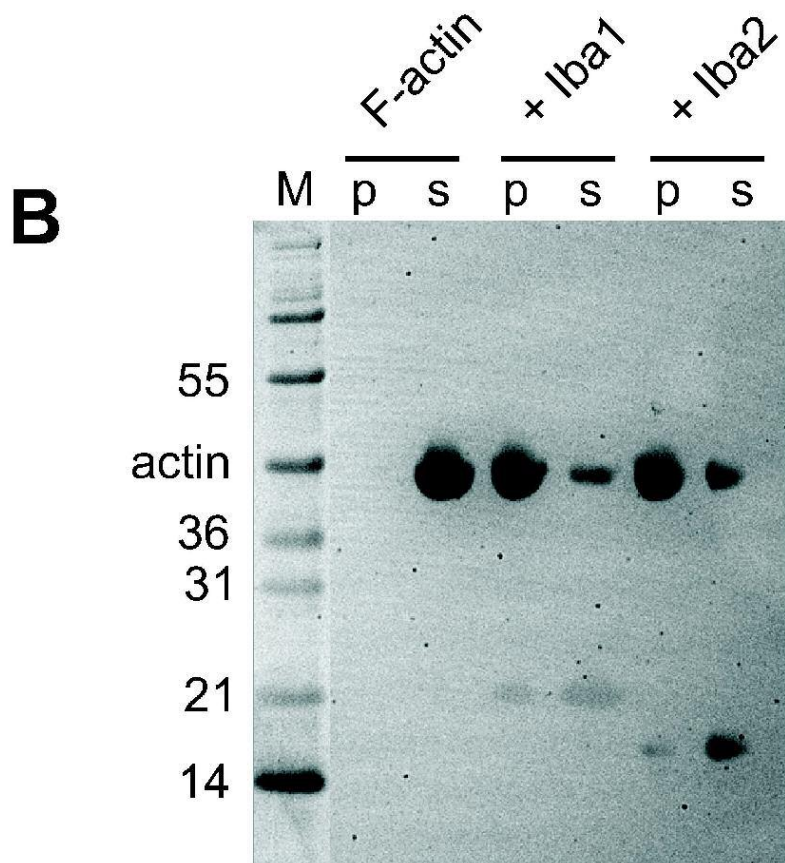
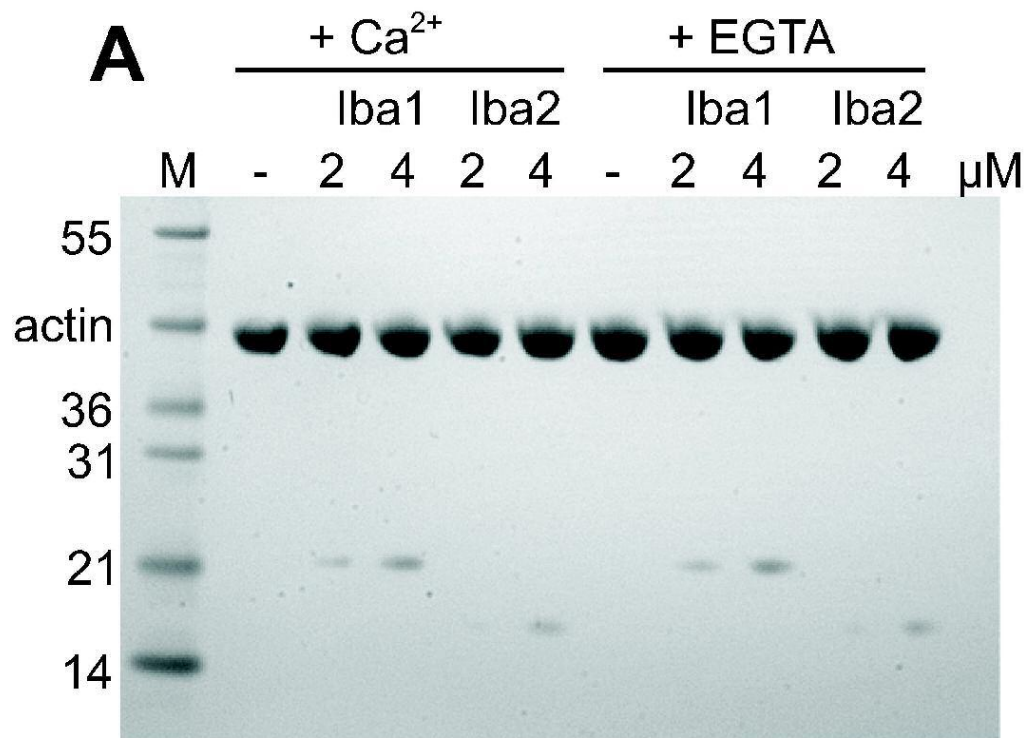


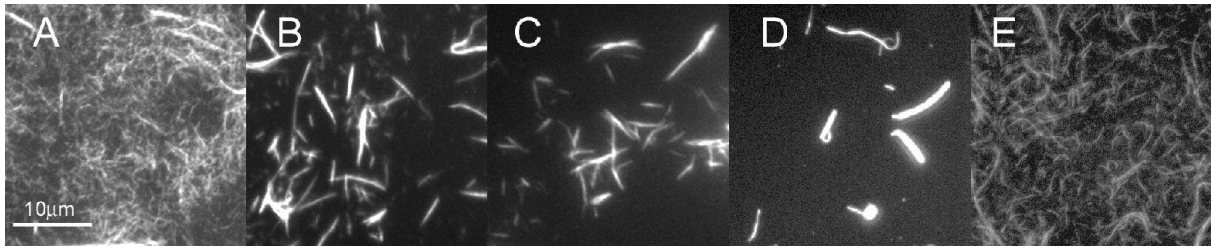
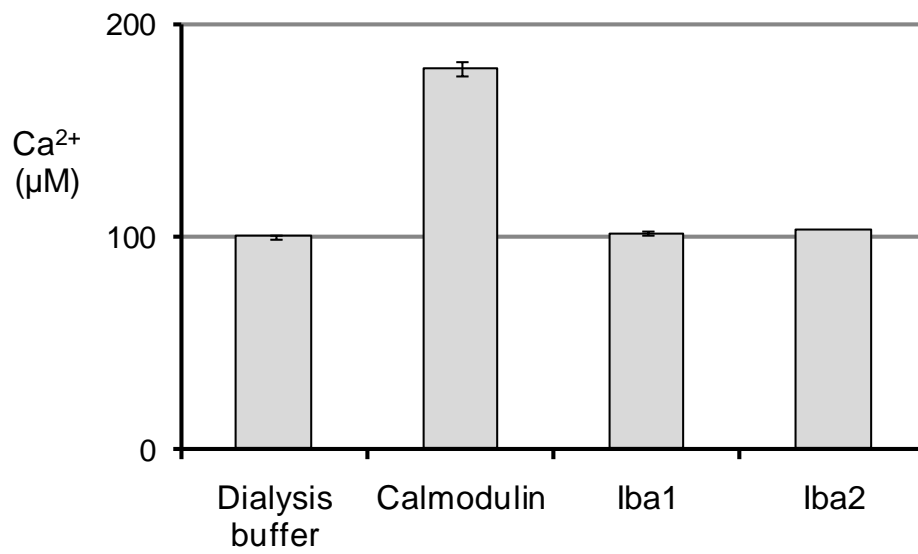
Figure 5**Figure 6**

Figure 7

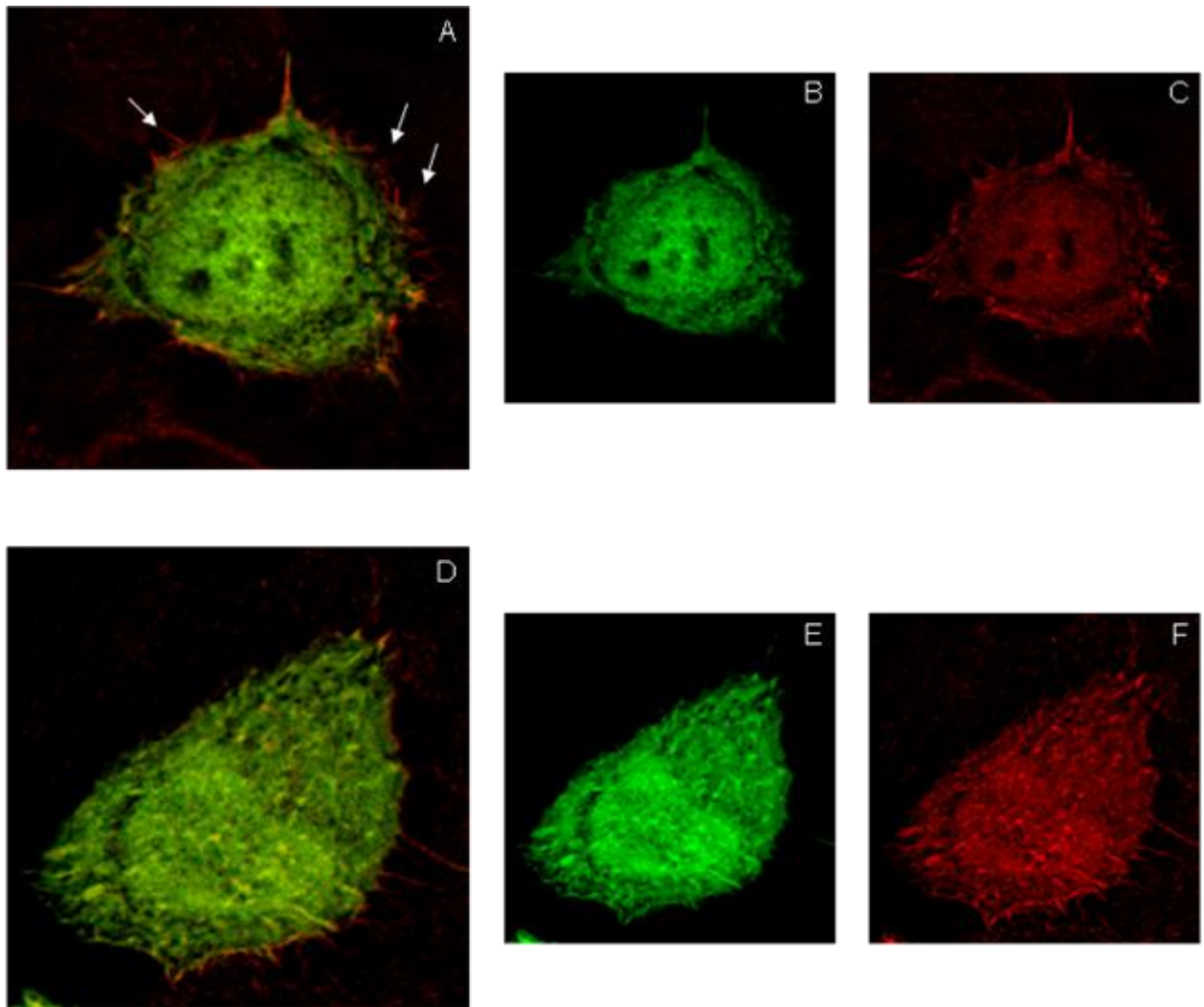


Figure 8

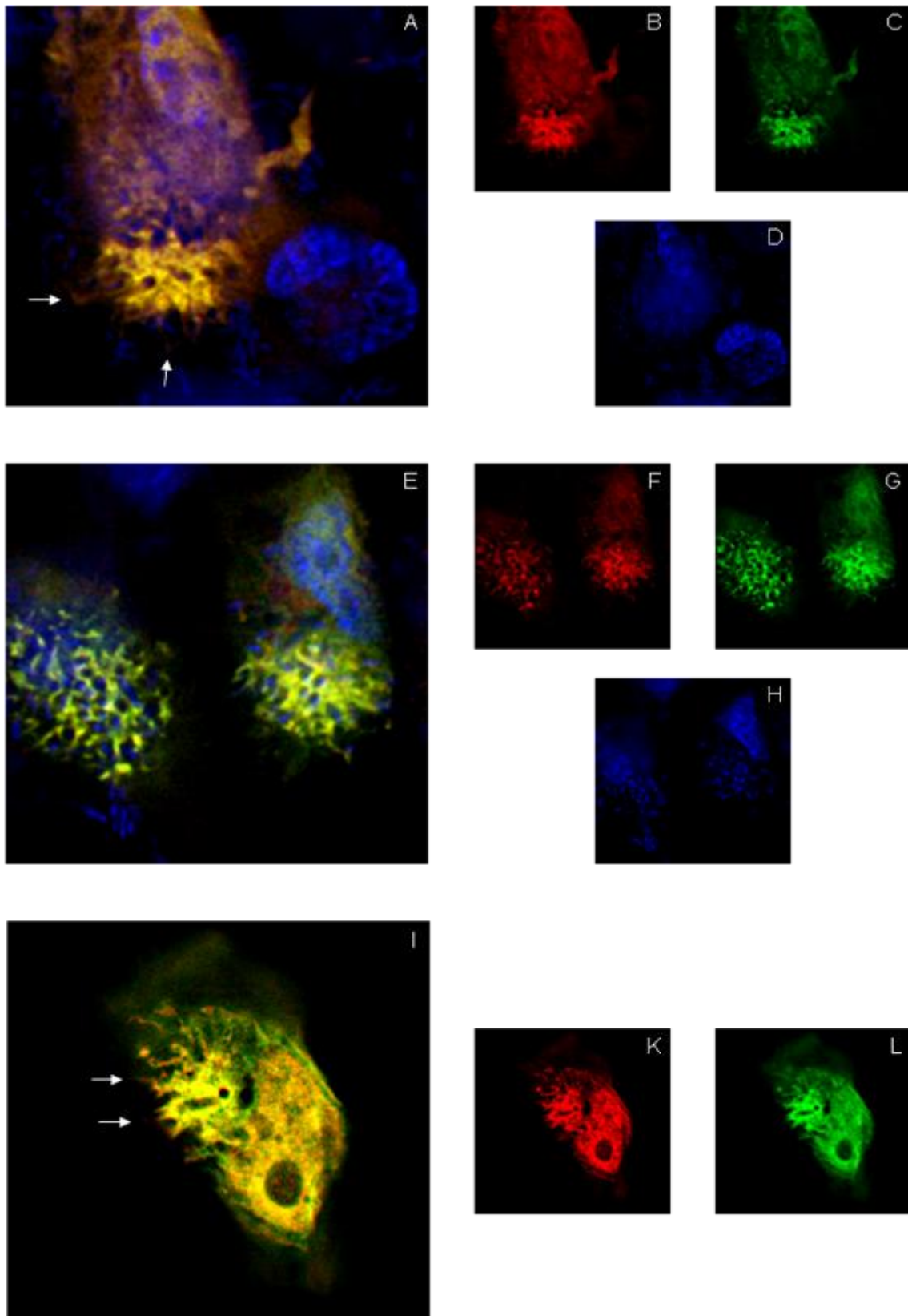


Figure 9

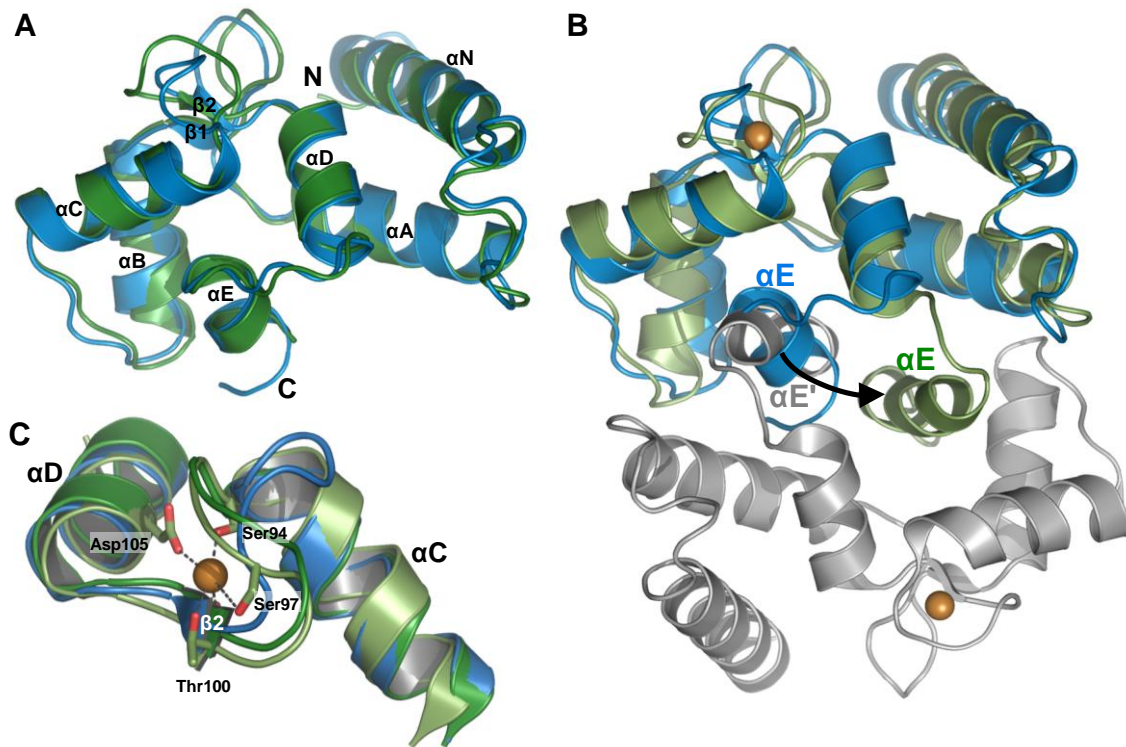


Figure 10

